Electronic Supplementary Material (ESI) for Journal of Materials Chemistry A.

Supporting Information

Increased power factors of organic-inorganic nanocomposite thermoelectric materials and the role of energy filtering

*Zhiming Liang,[1] Mathias J. Boland,[2] Kamal Butrouna,[1] Douglas R. Strachan,[2] and Kenneth R. Graham[1,]**

1. Z. Liang, Dr. K. Butrouna, Prof. K. R. Graham
Department of Chemistry, University of Kentucky, Lexington, Kentucky 40506, United States
E-mail: Kenneth.Graham@uky.edu

2. Dr. M. J. Boland, Prof. D. R. Strachan
Department of Physics & Astronomy, University of Kentucky, Lexington, Kentucky 40506, United States

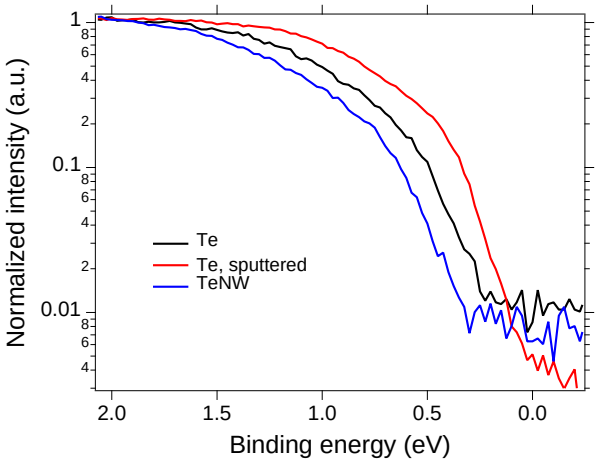

Figure S1: UPS spectra showing the valence band onset region of a tellurium thin film (Te), the same tellurium film after sputter cleaning, and tellurium nanowires on a semi logarithmic plot.

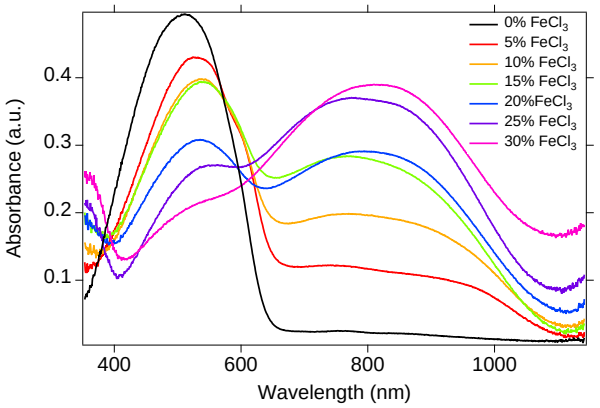

Figure S2: UV-VIS absorbance spectra of 5 to 30% $FeCl_3$ doped P3HT.

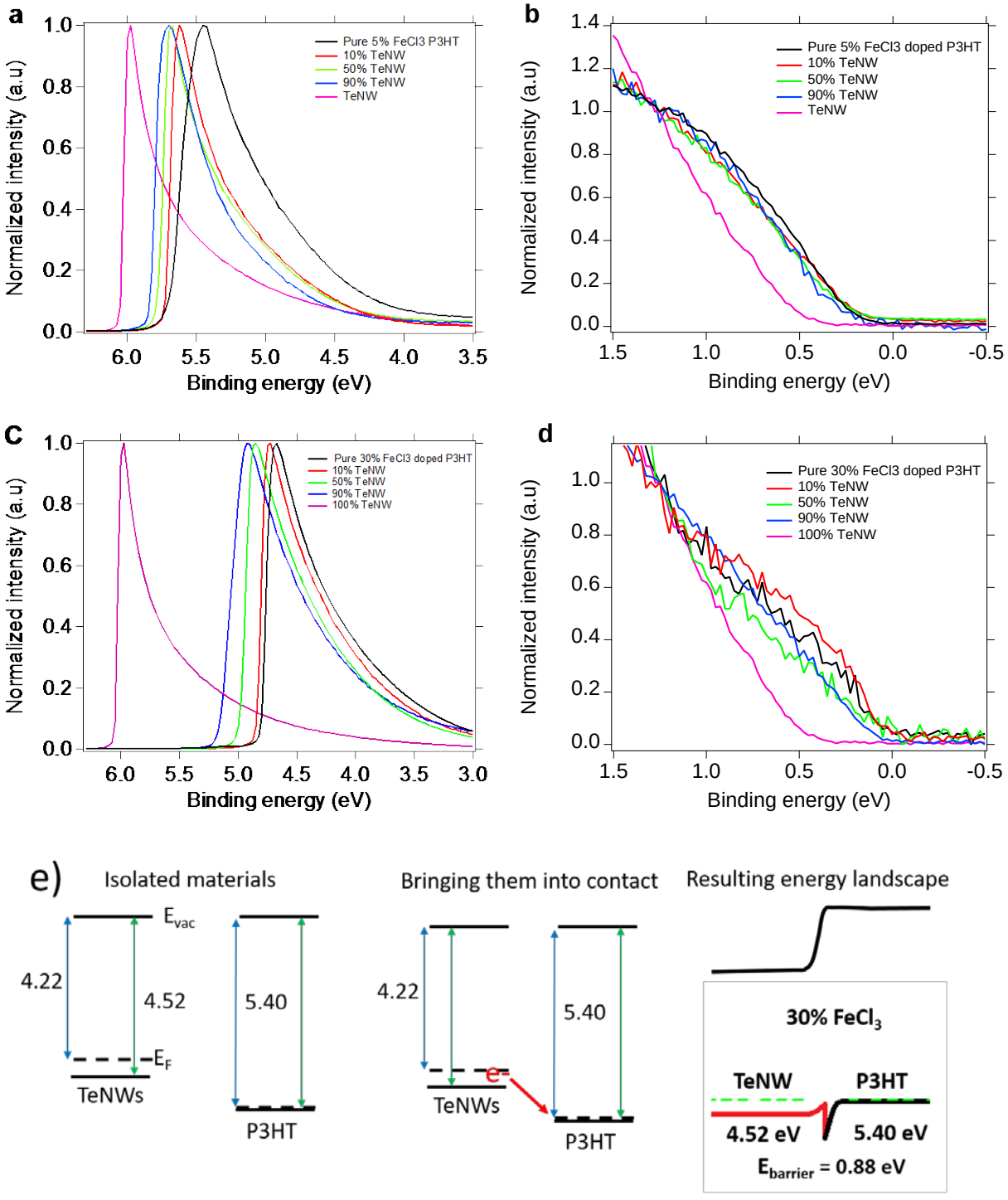

Figure S3. UPS spectra showing the secondary electron cut-off region (a, c) and the HOMO onset region (b, d) for 5 (a, b) and 30% (c,d) $FeCl_3$ doped blends with varying TeNW concentration. The origin of the energy landscape is shown in (e). E_{vac} and E_F are the vacuum and Fermi levels, respectively.

The UPS spectra shown in Figure S3 support the general trend in the energy barrier, i.e. it is significantly larger for the 30% $FeCl_3$ doped samples than the 5% doped samples. The spectra for the 50% P3HT:TeNW blends at both $FeCl_3$ concentrations show that the work functions and IEs are within 0.2 eV of their values for pure $FeCl_3$ doped P3HT. At 50% TeNW loading the TeNWs are nearly completely coated with P3HT, as the SEM images included in the main manuscript show that most of the TeNWs are coated even at 80% TeNW loading. Thus, the UPS results for the 50% TeNW films can be considered as analogous to TeNWs covered with a thin layer of P3HT. To illustrate how the interfacial energy landscape and barrier to charge transfer arises, we show the work function (blue lines) and IE (green lines) of pure TeNW films and pure 30% doped $FeCl_3$ films. As the P3HT is brought into contact with the TeNWs, electrons will transfer from the higher energy occupied electronic states (i.e. the states closer to the vacuum level) in the TeNWs to the available lower energy unoccupied electronic states in P3HT (P3HT is highly doped and thus there are many holes that can be filled), as indicated by the red arrow. As a result of this charge redistribution, the TeNW valence band bends towards the Fermi level at the TeNW/P3HT interface while the P3HT HOMO energy shifts away from the Fermi level at the TeNW/P3HT interface. Accompanying this charge redistribution is an upwards shift in the vacuum level, giving rise to the resulting energy landscape shown in Figure S3e. Assuming the starting work function (4.22) and IE for the pure TeNWs is the same in both the 5 and 30% $FeCl_3$ doped samples, and the work function of the 50% TeNW samples are 4.4 and 5.2 eV for the 5 and 30% $FeCl_3$ doped samples, it is apparent that the energy barrier for charge transfer is approximately 0.8 eV greater for the sample with 30% $FeCl_3$.

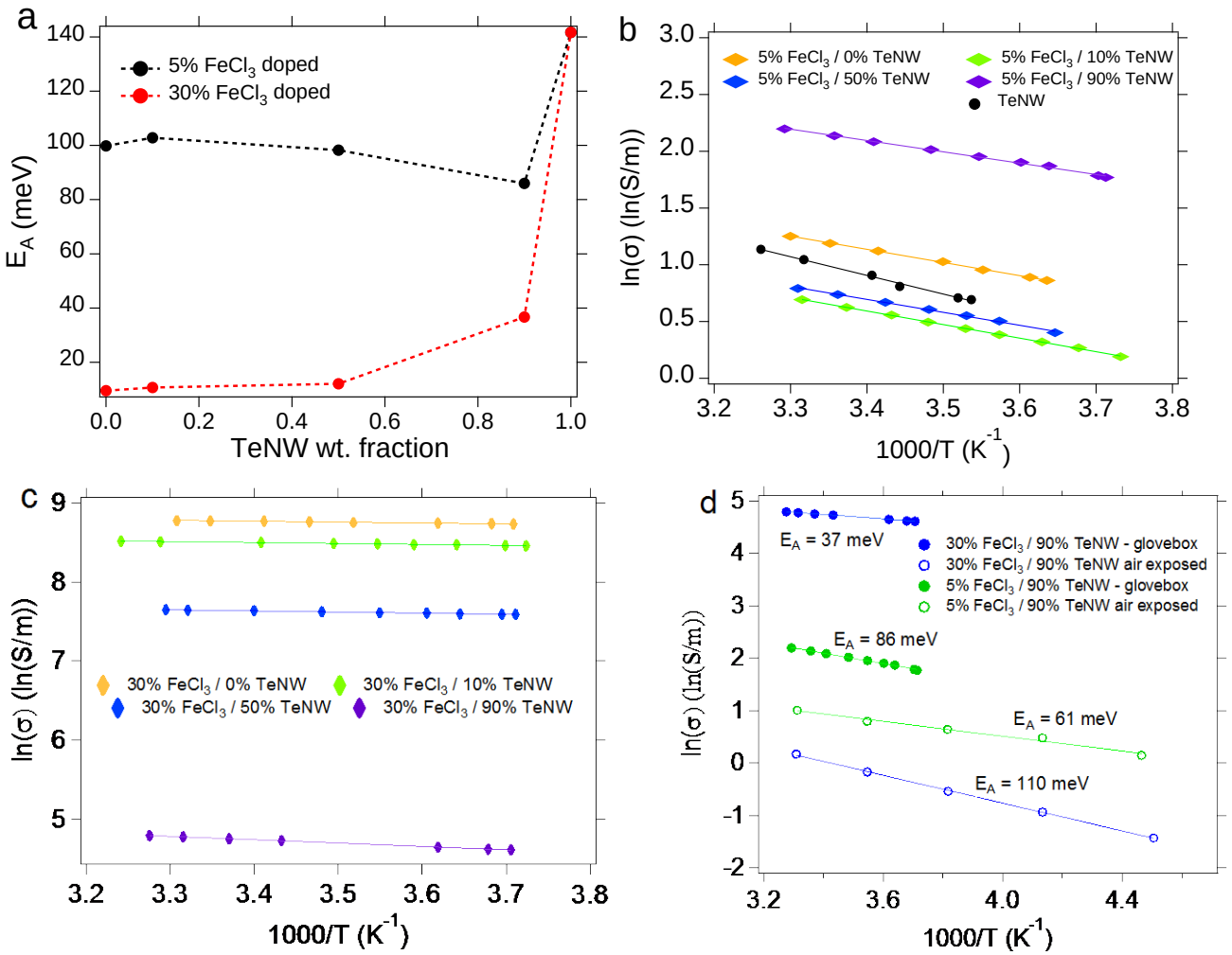

Figure S4. Activation energies for samples measured inside of our glovebox (a), temperature dependent electrical conductivity plots (b and c) measured inside of our glovebox and used to extract the activation energies for the P3HT:TeNW blends shown in a, and a comparison of the temperature dependent electrical conductivity measurements for 90% TeNW films performed in a probe station and in our glovebox (d), where the probe station measurements (labeled air exposed) involved unavoidable exposure to the ambient atmosphere and cooling to 77 K before beginning the measurements.

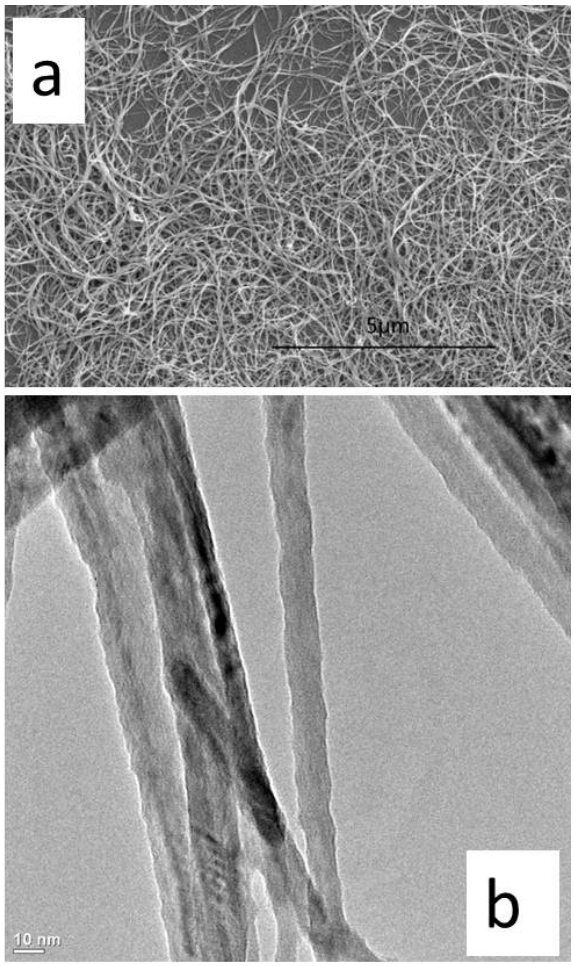

Figure S5: SEM (a) and TEM (b) images of the CTAB stabilized tellurium nanowires utilized in this work.

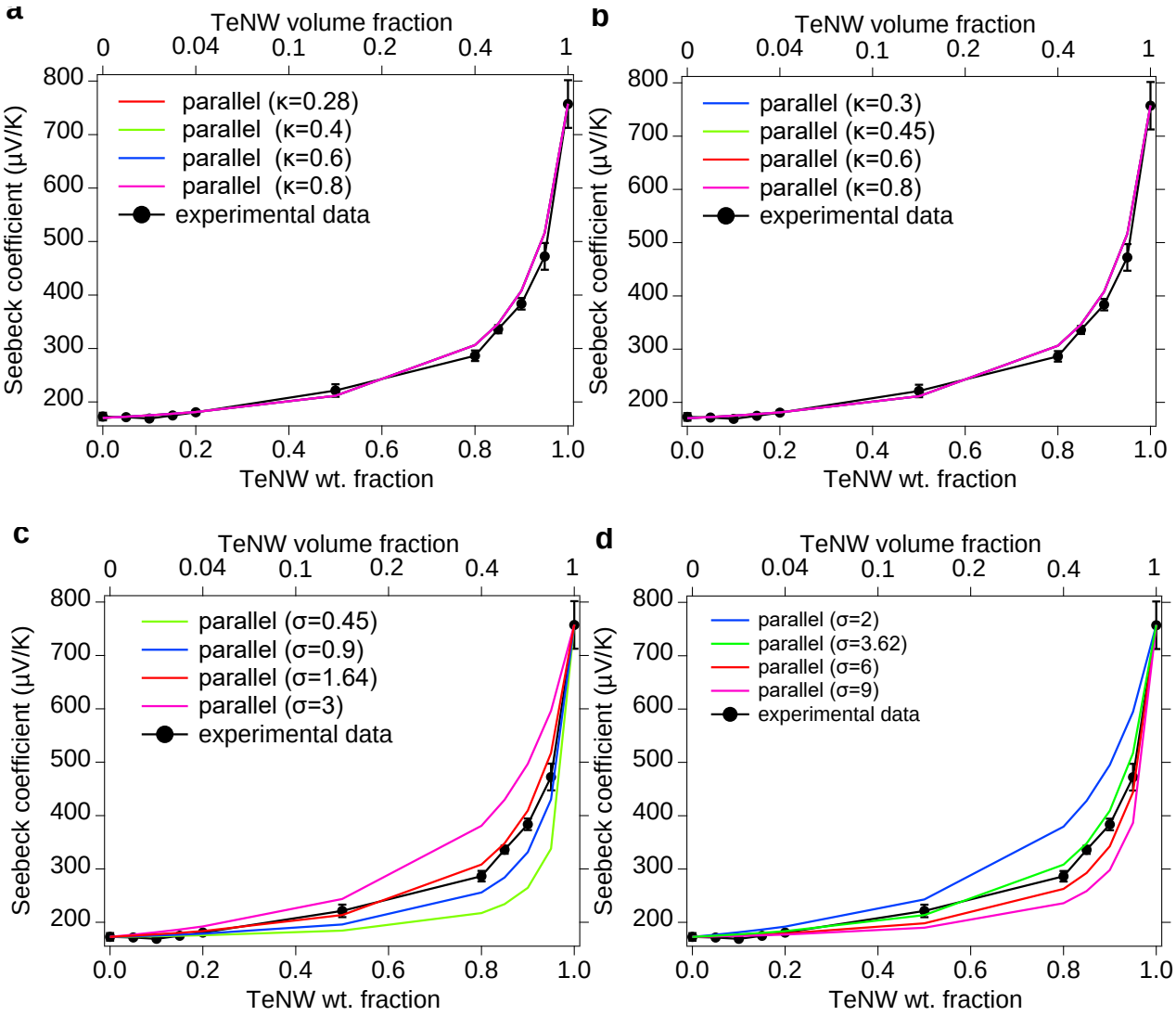

Figure S6: 5% $FeCl_3$ doped P3HT blends with varying TeNW loading showing how variations in the thermal conductivity (a,b) and electrical conductivity (c,d) of the TeNW (a,c) and P3HT (b,d) components influence how the pure parallel model fits the experimental data.

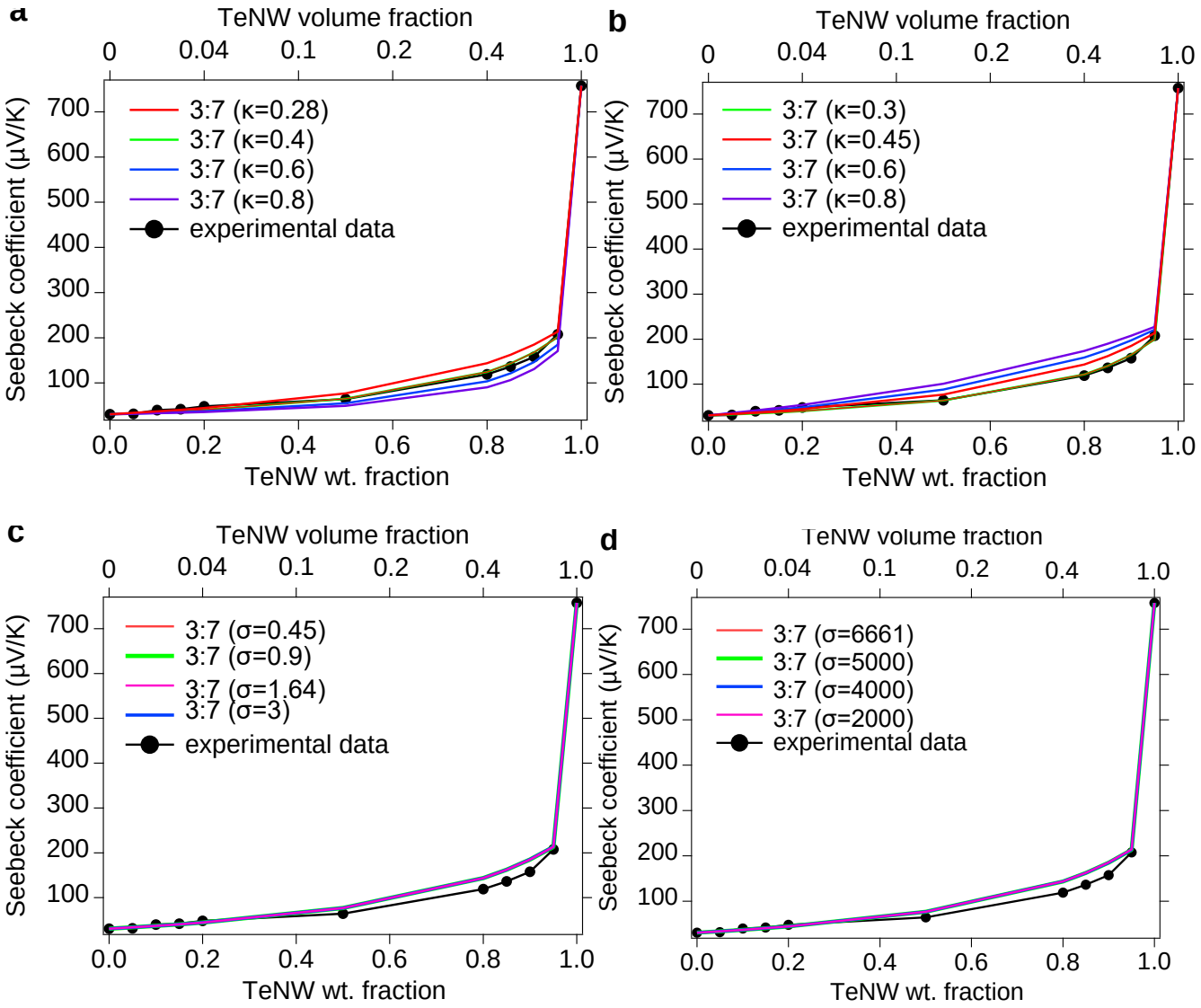

Figure S7: 30% $FeCl_3$ doped P3HT blends with varying TeNW loading showing how variations in the thermal conductivity (a,b) and electrical conductivity (c,d) of the TeNW (a,c) and P3HT (b,d) components influence how the 3:7 series:parallel model fits the experimental data.

Equation S1:[1]

$$W_D = \left[\frac{2N_{NW}\varepsilon_P\varepsilon_{NW}V_{bi}}{qN_P(\varepsilon_P N_P+\varepsilon_{NW}N_{NW})}\right]^{1/2} \qquad \text{(S1)}$$

Where V_{bi} is the built-in potential at equilibrium, N_{NW} and N_P are the charge-carrier concentrations in the TeNWs and P3HT, respectively, ε_{NW} and ε_P are the dielectric constants of Te and P3HT, W_D is the depletion width, and q is the elementary charge. In these calculations we use V_{bi}=0.08 V (5% $FeCl_3$

doped) and 0.88 V (30% $FeCl_3$ doped); $N_{NW}=1\times10^{18}$ cm^{-3};[2, 3] $N_P=2.7\times10^{19}$ cm^{-3} (5% $FeCl_3$ doped) and 1.6×10^{20} cm^{-3} (30% $FeCl_3$ doped);[4] $\varepsilon_P=3.1*10^{-11}(CV^{-1}cm^{-1})$;[5, 6] $\varepsilon_{NW}=2.43*10^{-10}(CV^{-1}cm^{-1})$;[7, 8] and $q=1.6*10^{-19}$ C.[1]

Equations S2 – S4:[9]

$$\sigma_{eff}(parallel) = x_1\sigma_1 + (1-x_1)\sigma_2 \qquad \text{(S2)}$$

$$\sigma_{eff}(series) = \frac{\sigma_1\sigma_2}{x_1\sigma_2 + (1-x_1)\sigma_1} \qquad \text{(S3)}$$

$$\sigma_{eff} = (x_1\sigma_1 + (1-x_1)\sigma_2)y + \frac{\sigma_1\sigma_2(1-y)}{x_1\sigma_2 + (1-x_1)\sigma_1} \qquad \text{(S4)}$$

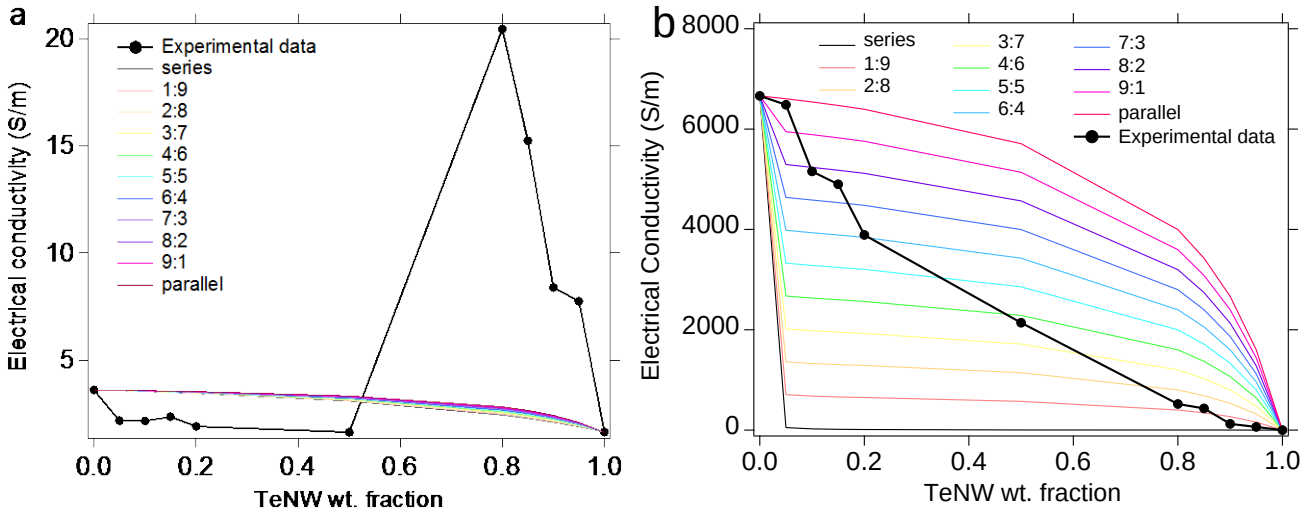

Figure S8: Combined series and parallel models of calculated and experimentally measured electrical conductivity for a) 5% $FeCl_3$ and b) 30% $FeCl_3$ doped P3HT:TeNW composites.

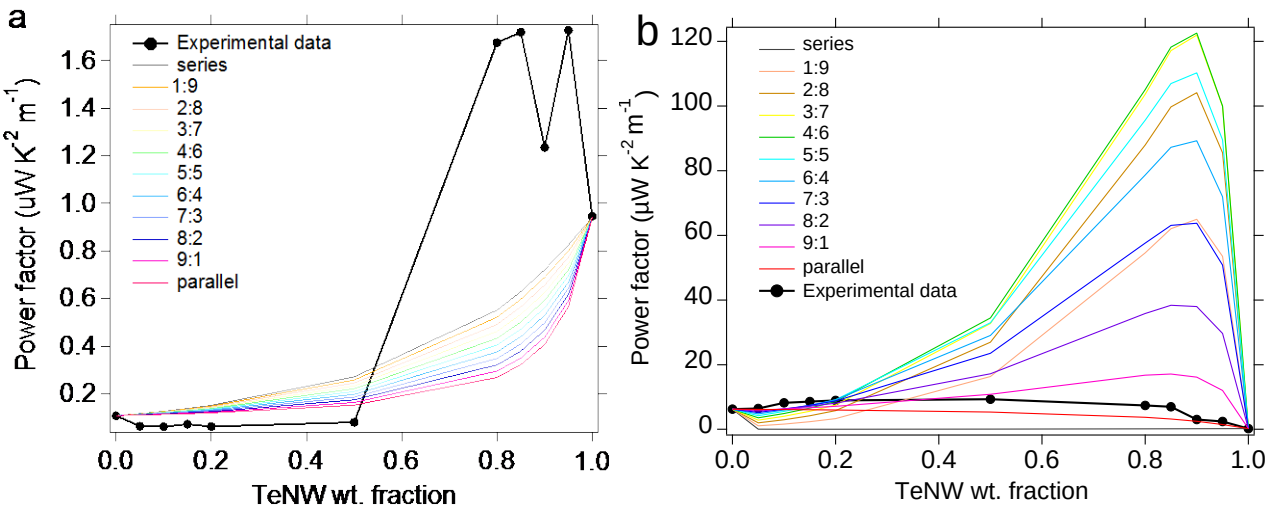

Figure S9: Combined series and parallel models of calculated and experimental power factor for a) 5% $FeCl_3$ and b) 30% $FeCl_3$ doped P3HT:TeNW composites.

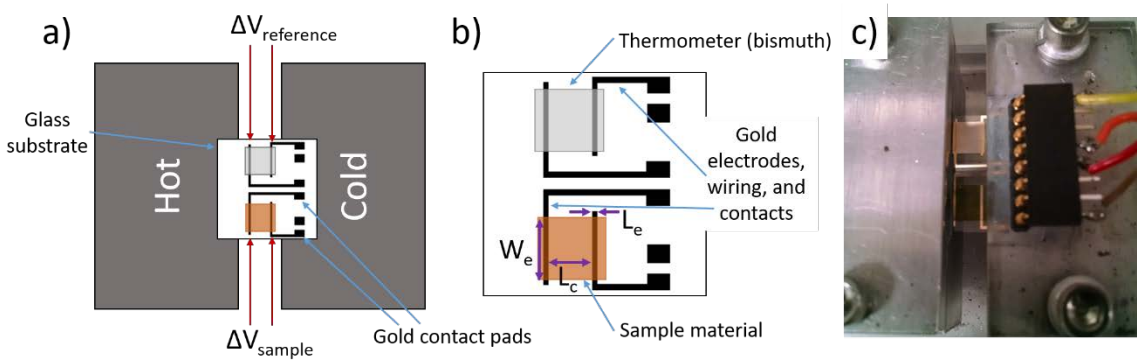

Figure S10. a) Overview schematic of our Seebeck measurement setup showing the substrate suspended between the hot and cold block, b) patterns of the sample, thermometer, and gold electrodes, and c) a photograph of the setup. In b) the critical dimensions are L_c = 4.0 mm, L_e = 0.4 mm, and W_e = 5.5 mm, which will result in an error of less than 8%.[10]

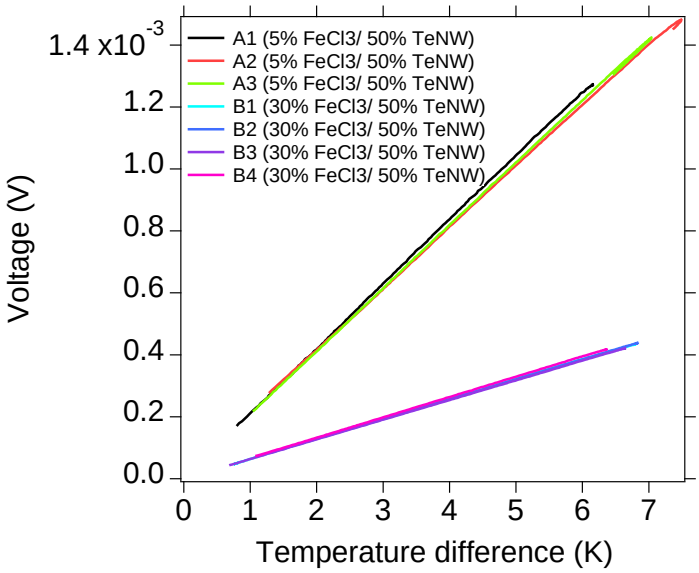

Figure S11. Sample voltage vs. temperature for 5 and 30% $FeCl_3$ doped samples with 50% TeNW concentration by weight. Each line corresponds with a separate film and is composed of approximately 200 individual data points. The temperature difference is calculated based on the bismuth film having a Seebeck coefficient of -64.4 μV/K.

References:

[1] S.M. Sze, K.-K. Ng, *Physics of Semiconductor Devices*, Third edition, Wiley-Interscience, Hoboken, NJ, USA **2007**.
[2] L.-B. Luo, F.-X. Liang, X.-L. Huang, T.-X. Yan, J.-G. Hu, Y.-Q. Yu, C.-Y. Wu, L. Wang, Z.-F. Zhu, Q. Li, J.-S. Jie, *J. Nanopart. Res.* **2012**, 14, 967.
[3] J. Choi, K. Lee, C. R. Park, H. Kim, *Carbon* **2015**, 94, 577.
[4] M. He, J. Ge, Z. Lin, X. Feng, X. Wang, H. Lu, Y. Yang, F. Qiu, *Energy Environ. Sci.* **2012**, 5, 8351.
[5] S. Chen, S.-W. Tsang, T.-H. Lai, J. R. Reynolds, F. So, *Adv. Mater.* **2014**, 26, 6125.
[6] S. Khelifi, K. Decock, J. Lauwaert, H. Vrielinck, D. Spoltore, F. Piersimoni, J. Manca, A. Belghachi, M. Burgelman, *J. Appl. Phys.* **2011**, 110, 094509.
[7] J. N. Hodgson, *J. Phys. Chem. Solids* **1962**, 23, 1737.
[8] K. F. Young, H. P. R. Frederikse, *J. Phys. Chem. Ref. Data* **1973**, 2, 313.
[9] Y. Gelbstein, *J. Appl. Phys.* **2009**, 105, 023713.
[10] S. V. Reenen, M. Kemerink, *Org. Electron.* **2014**, 15, 2250.